OPEN

General and Facile Surface Functionalization of Hydrophobic Nanocrystals with Poly(amino acid) for Cell Luminescence Imaging

Sheng Huang, Min Bai & Leyu Wang

State Key Laboratory of Chemical Resource Engineering, School of Science, Beijing University of Chemical Technology, Beijing 100029, China.

Hydrophobic nanocrystals with various shape, size, and chemical composition were successfully functionalized by poly(amino acid) with one particle per micelle without aggregation or precipitation via a facile, general, and low-cost strategy. Via simply tuning the pH value, multifunctional nanocomposites consisting of different nanocrystals were also fabricated. Due to the poly(amino acid) coating, these nanocrystals are highly water-stable, biocompatible, and bioconjugatable with chemical and biological moieties. Meanwhile, their shape, size, optical/magnetic properties are well retained, which is highly desirable for bioapplications. This developed strategy presents a novel opportunity to apply hydrophobic nanocrystals to various biomedical fields.

Inorganic nanocrystals (INCs) with excellent optical and magnetic properties, good crystallinity, controllable size, and uniform shape, have been successfully synthesized in organic solvents[1–4]. However, due to the hydrophobic surface[5–7], their bioapplications are greatly limited. So, surface functionalization of these INCs is prerequisite for biomedical applications, not only to render them reasonably water dispersible and biocompatible, but also to provide active sites for subsequent functional conjugation with biological or chemical moieties[8–14]. In some cases, small particle size and good water-stability of the nanobiotag is highly expected especially for the intracellular tracking of biomolecules[5,15–18]. Therefore, the particle size, shape, and optical/magnetic properties should be kept unchanged after the functionalization. To date, ligand exchange is still a general way to tailor the surface of hydrophobic INCs[19–21], especially for quantum dots (QDs)[17,22], although it often compromises the luminescence efficiency and photochemical stability due to the detachment of small molecule ligands from the surface of the luminescent nanoparticles (NPs). To increase the binding stability, multidentate ligands were used to functionalize the quantum dots (QDs)[23–25]. Silanization, another coating method, is highly reproducible and can be applied to various NPs[18,26,27], but it is time-consuming and the particle size has obvious increase after silica coating. In addition, encapsulation with amphiphilic polymers[12,28–30] and lipids[15,31,32] is another strategy for the functionalization of hydrophobic INCs, but the amphiphilic block polymer is usually synthetic and thus its biocompatibility[8] and biodegradability need further improvement. Based on the oil phase evaporation-induced self-assembly, hydrophobic INCs were successfully transferred into hydrophilic nanospheres[33–38]. Sometimes, the surfactants such as triton TX-100[39] and cytotoxic hexadecyltrimethy ammonium bromide (CTAB) are usually necessary. The large particle size and cytotoxicity partly limit the biomedical applications of these nanocomposites[40,41]. Therefore, it would be of particular interest to develop a facile and general strategy to embed the hydrophobic INCs with various shape, size and chemical composition into biomacromolecule micelles with one particle per micelle, little increase of hydrodynamic size, and well retained optical/magnetic properties.

Results

Herein, we report a facile and general strategy to functionalize hydrophobic INCs with various shape, size and chemical composition (Figure 1). It is notable that, thanks to its super biocompatibility, negligible side effects, and inappreciable antigenicity in the human body, polyaspartic acid (PASP), a poly-(amino acid), has become a new type of water-soluble and biodegradable functional material for drug delivery and encapsulation of NPs[42–45]. Due to the poly(amino acid) coating, these nanocrystals are highly water-stable, biocompatible, and bioconjugatable
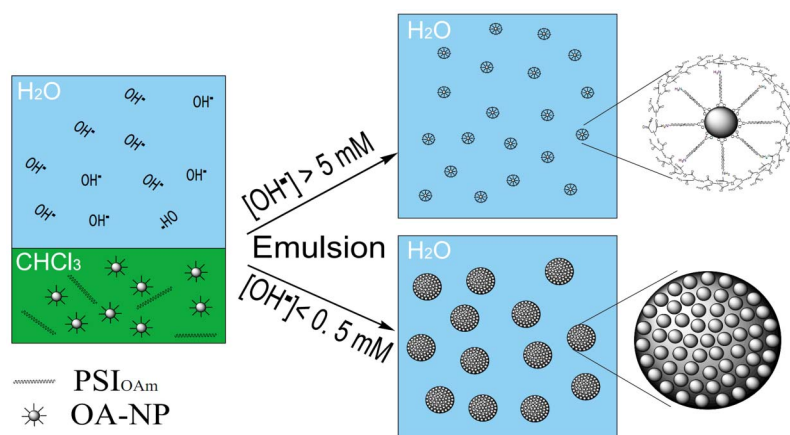
Figure 1 | Scheme for the fabrication of individual NPs (top) and multifunctional nanocomposites (bottom) with hydrophilic and biocompatible surface employing poly(amino acid) as coating agents by simply tuning pH value. OA: oleic acid; NP: nanoparticle; PSI_{OAm}: oleylamine-modified poly-succinimide.

with chemical and biological moieties. Meanwhile, their shape, size, optical/magnetic properties are well retained, which is highly desirable for bioapplications[46,47].

As shown in Figure S1, the lactam ring in the poly-succinimide (PSI) chain is easily opened via aminolysis by oleylamine to form PASP derivatives with a side-chain functional group, and followed by hydrolysis of the remaining succinimide units in the PSI backbone in alkaline aqueous solution. Herein, 30% succinimide units in PSI were aminolysed by oleylamine to form PSI_{OAm} that is soluble in chloroform but not in water. To transfer the hydrophobic INCs into water, the mixture chloroform solution containing PSI_{OAm} and hydrophobic INCs was mixed with NaOH aqueous solution by means of ultrasonication. The hydrophobic nanocrystal was then encapsulated in the amphiphilic PSI_{OAm} micelle, forming the oil-in-water (O/W) emulsion (Figure 1). After the evaporation of chloroform, hydrophilic and individual nanocrystal was obtained. During this process, the PSI_{OAm} tends to assemble onto the individual hydrophobic INC surface as a thin layer through van de Waals interaction between alkyl chains of oleylamine in PSI_{OAm} and oleic acid on hydrophobic NPs (Figure S2). Meanwhile, after hydrolyzation under basic conditions, the carboxylic groups in the PSI_{OAm} render the INCs not only highly water stable but also bioconjugatable with chemical and biological moieties. To testify the feasibility of this method, hydrophobic noble metal (Ag, $\sim$8 nm), quantum dots (ZnS:Mn^{2+}, $\sim$7 nm), magnetic oxides (Fe_3O_4, $\sim$11 nm), downconversion (DC) (LaF_3:Ce^{3+}/Tb^{3+}, $\sim$10 nm), and upconversion (UC) luminescence fluorides (NaYF$_4$:Yb^{3+}/Er^{3+}, $\sim$14 nm) were transferred into water, respectively. As shown in Figure 2, all the hydrophobic NPs with various shape, size and chemical composition were successfully encapsulated into the PSI_{OAm}-COO^- micelle with one particle per micelle. From the transmission electron microscopy (TEM) images, it is clear that the particle size and shape have no obvious change after the surface modification, and no aggregation can be observed. Also, hydrophobic NaYF$_4$:Yb^{3+}/Er^{3+} ($\sim$29 nm) nanorods and YPO$_4$ ($\sim$36 nm) nanoplates have been successfully encapsulated (Figure S3). Moreover, as shown in the photos of Figure 2, the properties including luminescence and magnetism were well maintained after functionalization.

For the fabrication of mono- or multi-components nanocomposites (NCs), we construct a larger micelle containing plenty of NPs in spite of their composition by only decreasing the concentration of OH^- and thus the ratio of hydrophilic to hydrophobic groups, i.e. the ratio of carboxyl to oleylamine (OAm) in the PSI_{OAm} chain. Thanks to the decreasing of hydrophilic segments in the PSI_{OAm} chain, after evaporating the chloroform, the hydrophobic NPs are forced to assemble densely into a nanosphere coated with PSI_{OAm} and keep

stable in water. In this work, as representatives, ZnS:Mn^{2+}, ZnS:Mn^{2+}-NaYF$_4$:Yb^{3+}/Er^{3+}, and ZnS:Mn^{2+}-Fe_3O_4 NCs were constructed to verify the generality of this fabrication technology. As shown in the TEM images of Figure 3, the as-prepared NCs are spheric in shape with the size of 100–200 nm. Compared to the darker contrast of inorganic NPs, the polymer shell with a low contrast can be observed clearly. After the formation of ZnS:Mn^{2+} NCs,
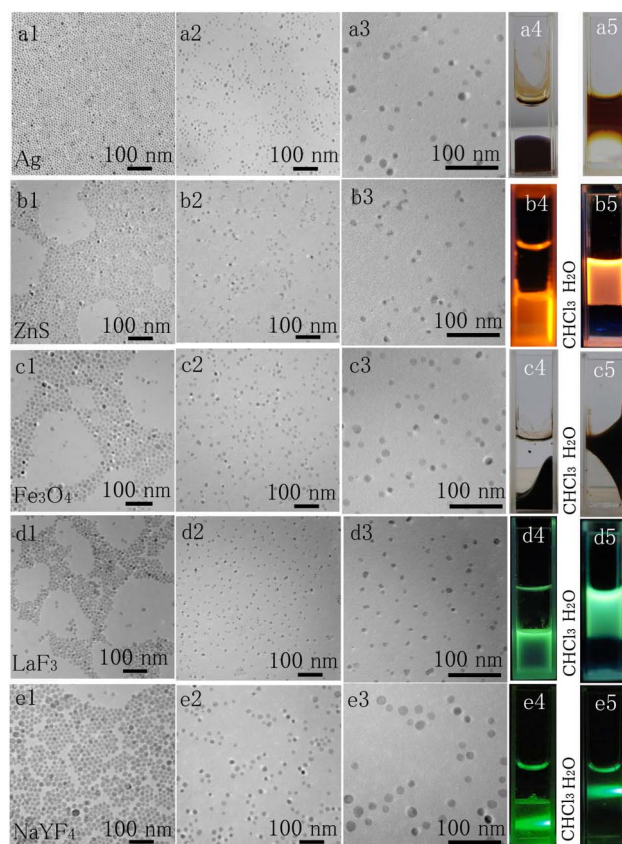

Figure 2 | TEM images (1, 2, 3) and photographs (4, 5) of the inorganic nanocrystals before (1, 4) and after (2, 3, 5) surface modification. Photograph 4 and 5: the top layer is water and the bottom layer is chloroform; a) daylight; b, d) 254 nm UV light; c) daylight and magnet; e) 980-nm diode laser. (a) Ag; (b) ZnS:Mn^{2+}; (c) Fe_3O_4; (d) LaF_3:Ce^{3+}/Tb^{3+}; (e) NaYF$_4$:Yb^{3+}/Er^{3+}. TEM image: image 3 is the image of 2 with larger magnification.

2
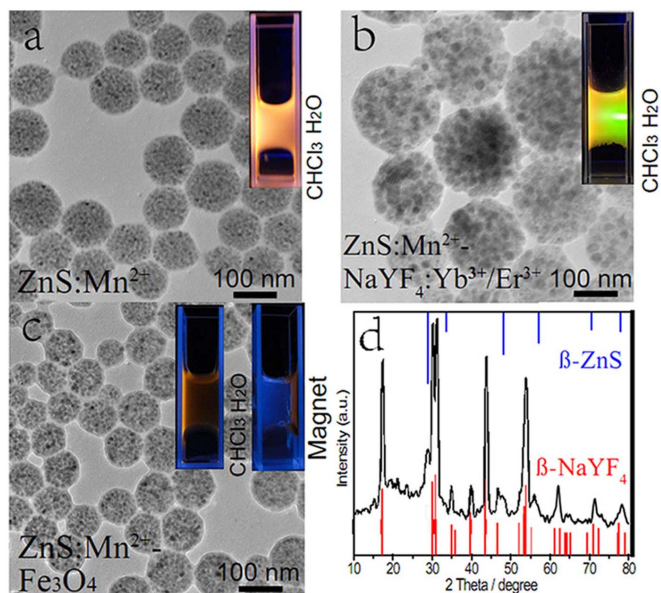
Figure 3 | TEM images of (a) ZnS:Mn²⁺, (b) ZnS:Mn²⁺-NaYF₄:Yb³⁺/Er³⁺ and (c) ZnS:Mn²⁺-Fe₃O₄ NCs. (d) X-ray diffraction (XRD) pattern of ZnS:Mn²⁺-NaYF₄:Yb³⁺/Er³⁺ NCs. Insets: Digital photos of the NCs dispersed in water under irradiation. The top and bottom layer are water and chloroform, respectively. a) 254 nm UV light; b) 254 nm UV light and 980 nm NIR laser; c) 254 nm UV light and external magnet on the right side of the cuvette.

the orange fluorescence of ZnS:Mn²⁺ is preserved very well (inset of Figure 3a). For the ZnS:Mn²⁺-NaYF₄:Yb³⁺/Er³⁺ NCs, both the orange fluorescence of ZnS:Mn²⁺ and the green upconversion luminescence of NaYF₄:Yb³⁺/Er³⁺ can be observed under the irradiation of both UV light (254 nm) and NIR (980 nm) diode laser (inset of Figure 3b), rendering the NCs desirable for DC-UC dual-modal luminescence imaging application. However, for the ZnS:Mn²⁺-Fe₃O₄ fluorescent-magnetic NCs, due to the absorption of black magnetite, the NCs demonstrate dull-red fluorescence. These NCs are easily drawn to the side wall when an assistant magnet is adjoined to the cuvette (inset of Figure 3c). The composition of the ZnS:Mn²⁺-NaYF₄:Yb³⁺/Er³⁺ NCs is not only characterized from the TEM image and dual-modal luminescence but also identified by the X-ray diffraction (XRD) results show in Figure 3d. The results indicate that the current method is also useful for the fabrication of multifunctional NCs and is highly desirable for the preparation of barcode microbeads for multimodal imaging.

Discussion

The poly(amino acid) coating was characterized with FITR (Figure 4). The characteristic peaks of lactam ring around 1789 and 1708 cm⁻¹ for $\upsilon_{(C=O)}$ were observed on PSI$_{OAm}$ (Figure 4b), but weaken on the surface of NaYF₄:Yb³⁺/Er³⁺@PSI$_{OAm}$-COO⁻ (Figure 4c), because most of the lactam ring were hydrolyzed to carboxylic groups, in agreement with the peak of 1712 cm⁻¹ for NaYF₄:Yb³⁺/Er³⁺@PSI$_{OAm}$-COO⁻ (Figure 4c). The other vibration peaks in spectrum c (Figure 4c) are in accordance with those in b (Figure 4b), indicating that the PSI$_{OAm}$ have been coated onto the nanoparticles. The characteristic vibration adsorption peaks of lactam ring and carboxylic group can not be observed from spectrum a (Figure 4a), further suggesting the PSI$_{OAm}$-COO⁻ coating is successful.

The dynamic light scattering (DLS) results indicate that the particle size of NaYF₄:Yb³⁺/Er³⁺ and ZnS:Mn²⁺ NPs has no obvious change before (NaYF₄:Yb³⁺/Er³⁺ NPs 19.2±2.9 nm; ZnS:Mn²⁺ NPs 8.2±2.0 nm in cyclohexane) and after (NaYF₄:Yb³⁺/Er³⁺ NPs

22.0±4.3 nm; ZnS:Mn²⁺ NPs 9.8±3.0 in water) the encapsulation (Figure 5). The slight increase in the particle size can be attributed to the PSI$_{OAm}$ coating. The results indicate that no aggregation is formed after the encapsulation, and each PASP micelle has only one particle, which is very important for intracellular tracking of biomolecules.

In order to investigate the potential biomedical applications of the individual NaYF₄:Yb³⁺/Er³⁺ NPs and ZnS:Mn²⁺ NPs as candidates of luminescent bio-tags, we first examine their cytotoxicity by the MTT cell proliferation assay. As shown in Figure 6, when incubated with 100 μg/mL of NaYF₄:Yb³⁺/Er³⁺ NPs or ZnS:Mn²⁺ NPs for 24 h,

Figure 4 | FTIR spectra of the (a) oleic acid (OA)-coated NaYF₄:Yb³⁺/Er³⁺, (b) PSI$_{OAm}$, and (c) NaYF₄:Yb³⁺/Er³⁺@PSI$_{OAm}$-COO⁻.
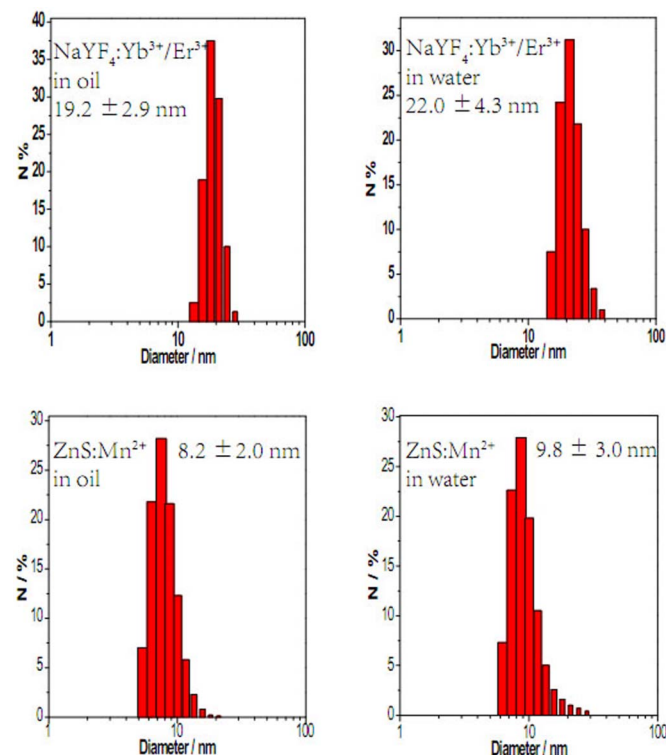
Figure 5 | Size distribution profiles obtained by dynamic light scattering (DLS) for NaYF₄:Yb³⁺/Er³⁺ and ZnS:Mn²⁺ before (left, in cyclohexane) and after (right, in water) the surface modification.
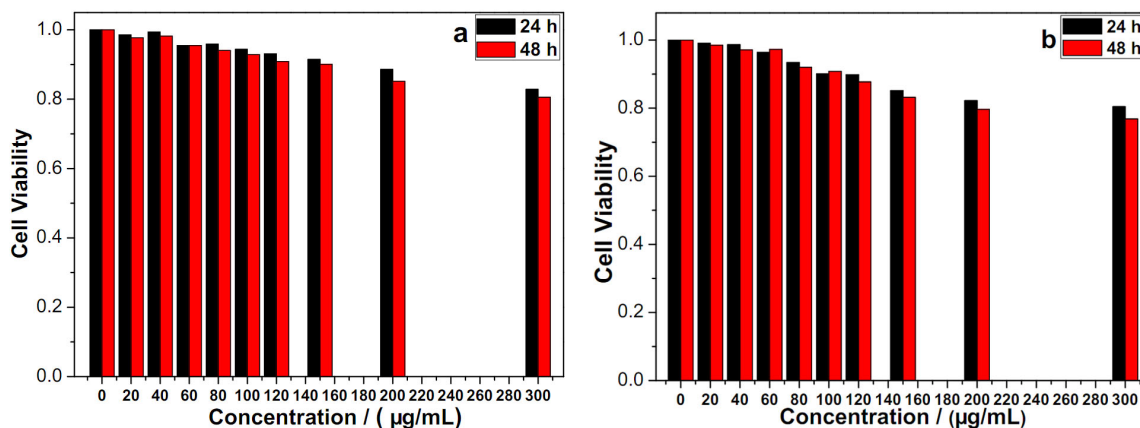
Figure 6 | Cell viability tests of surface functionalized NaYF₄:Yb³⁺/Er³⁺ NPs (a) and ZnS:Mn²⁺ NPs (b) on HeLa cell line at different concentration after incubation for 24 (black) and 48 h (red), respectively.

the viability of HeLa cells was still over 94% and 90%, respectively. Even though the concentration is up to 300 μg/mL, over 80% cells are still alive after incubation for 48 h, suggesting a very good biocompatability of the INPs after surface modification.

To render the luminescent NPs specifically recognize the overexpressed receptor of folic acids (FA) on the HeLa cells[48], these two kinds of NPs were bioconjugated with FA before incubation with

the cells for luminescence imaging. Figure 7 depicted the imaging results of the HeLa cells incubated with individual NaYF₄:Yb³⁺/Er³⁺ and ZnS:Mn²⁺ NPs, respectively. As can be seen from these images, the FA-conjugated NPs could specifically label the HeLa cells (Figure 7 b and d). As a control, even incubated with the cells via the same recipe as above, the bare NPs without FA, could not stain the HeLa cells in spite of their hydrophilic surface (Figure 7a and c). Interestingly, strong green UC emission was only observed from the cell membrane (Figure 7b3), indicating that no nonspecific binding on the cell membrane and endocytosis of NPs has happened. On the other hand, red signal (Figure 7d3) is from DC fluorescence of ZnS:Mn²⁺ (Figure 7d2), further revealing the specific grafting of NPs onto the cell surface. Owing to their small hydrodynamic size and good dispersibility, NPs distributed homogeneously on the cell surface, which have the similar dying effect as cytomembrane dyes.

In summary, we have successfully developed a facile, general, and low cost strategy for the surface functionalization of hydrophobic INCs with various shape, size, and chemical composition via poly (amino acid) coating. This functionalization has no obvious effects on the size, shape, and optical/magnetic properties of the INCs. By simply tuning the pH value, this novel strategy has also been successfully applied for the fabrication of multifunctional nanocomposites. The functionalized NPs are highly water stable, biocompatible, and bioconjugatable. The cell imaging results demonstrated that these poly(-amino acid) coated NPs are of great potential for biomedical applications. The current work paves the way to the surface modification of hydrophobic NPs, which will draw great interests from the fields of chemistry, materials, nanobiotechnology, and nanomedicine.
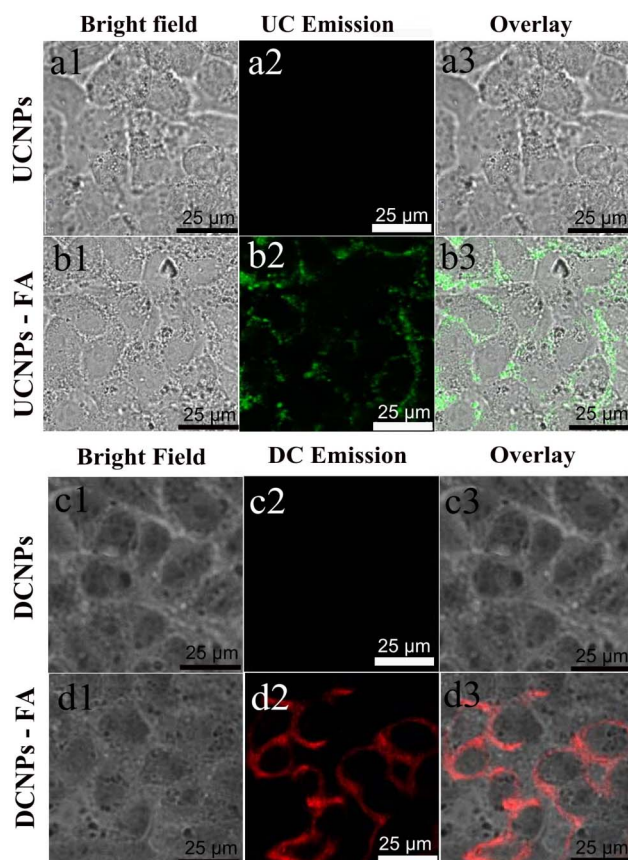

Figure 7 | Confocal luminescence imaging of HeLa cells stained with (a) NaYF₄:Yb³⁺/Er³⁺@PSI_{OAm}-COO⁻ NPs, (b) NaYF₄:Yb³⁺/Er³⁺@PSI_{OAm}-COO⁻@FA NPs, (c) ZnS:Mn²⁺@PSI_{OAm}-COO⁻ NPs and (d) ZnS:Mn²⁺@PSI_{OAm}-COO⁻@FA NPs. Particle concentration: 100 μg/mL. Irradiation: (a2, b2) 980 nm for NaYF₄:Yb³⁺/Er³⁺; (c2 and d2) ~360 nm for ZnS:Mn²⁺.

Methods

Preparation of PSI_{OAm}. 1.6 g of polysuccinimide (PSI) was dissolved in 32 mL of N, N-Dimethylformamide (DMF) at 60°C under magnetic stirring followed by the addition of oleylamine (1.63 mL). The mixture was treated at 100°C for 5 h before cooling to room temperature. Then methanol (80 mL) was added to precipitate the product (PSI_{OAm}). Finally, the PSI_{OAm} was redispersed into chloroform to get a stock solution with concentration of 190 mg/mL after centrifugation and then evaporating the trace amount of residual methanol.

Fabrication of hydrophilic individual NPs and multifunctional nanocomposites. Taking NaYF₄:Yb³⁺/Er³⁺ NPs as an example, into 10 mL of NaOH (5.0 mM)ee aqueous solution, 1.0 mL of mixture chloroform solution of PSI_{OAm} (38 mg) and NaYF₄:Yb³⁺/Er³⁺ NPs (5.0 mg) was added under ultrasonication (350 W, 6 min) and stirring. Subsequently, the chloroform was removed by evaporating at 55°C for 30 min. The hydrophilic nanocrystals were collected and purified by centrifugation at 11000 rpm for 20 min and redispersed into water (3 mL). It should be mentioned that the dosage of different NPs is tuned according to the size of NPs. Generally, small NPs need more PSI_{OAm} due to their larger specific surface area. For the nanocomposites, taking ZnS:Mn²⁺-NaYF₄:Yb³⁺/Er³⁺ NCs as an example, into 10 mL of NaOH (0.5 mM) aqueous solution, 1.0 mL of chloroform colloidal solution containing PSI_{OAm} (38 mg), ZnS:Mn²⁺ NPs (7 mg) and NaYF₄:Yb³⁺/Er³⁺ NPs (2.5 mg) was added under ultrasonication (350 W, 6 min) and stirring. Then the obtained NCs was purified and collected as above. Moreover, the molecular weight (M_w) of

PSI$_{OAm}$-COOH (after aminolysis and hydrolysis) was 7958 with a Polydispersity (PD) of 1.03, which was determined by a 4800 Plus MALDI TOF/TOF mass spectrometer (Figure S4).

1. Wang, X., Zhuang, J., Peng, Q. & Li, Y. D. A general strategy for nanocrystal synthesis. *Nature* **437**, 121–124 (2005).
2. Puntes, V. F., Krishnan, K. M. & Alivisatos, A. P. Colloidal nanocrystal shape and size control: The case of cobalt. *Science* **291**, 2115–2117 (2001).
3. Sun, S. H., Murray, C. B., Weller, D., Folks, L. & Moser, A. Monodisperse FePt nanoparticles and ferromagnetic FePt nanocrystal superlattices. *Science* **287**, 1989–1992 (2000).
4. Yin, Y. & Alivisatos, A. P. Colloidal nanocrystal synthesis and the organic-inorganic interface. *Nature* **437**, 664–670 (2005).
5. Deng, M. L., Ma, Y. X., Huang, S., Hu, G. F. & Wang, L. Y. Monodisperse upconversion NaYF$_4$ nanocrystals: syntheses and bioapplications. *Nano Res.* **4**, 685–694 (2011).
6. Wang, L. Y. & Li, Y. D. Controlled synthesis and luminescence of lanthanide doped NaYF4 nanocrystals. *Chem. Mat.* **19**, 727–734 (2007).
7. Wang, L. Y. & Li, Y. D. Na(Y$_{1.5}$Na$_{0.5}$)F$_6$ single-crystal nanorods as multicolor luminescent materials. *Nano Lett.* **6**, 1645–1649 (2006).
8. Chen, E. Y. *et al.* Functionalized carboxyl nanoparticles enhance mucus dispersion and hydration. *Sci. Rep.* **2**, 211; DOI: 10.1038/srep00211 (2012).
9. Michalet, X. *et al.* Quantum dots for live cells, in vivo imaging, and diagnostics. *Science* **307**, 538–544 (2005).
10. Medintz, I. L. *et al.* Quantum-dot/dopamine bioconjugates function as redox coupled assemblies for in vitro and intracellular pH sensing. *Nat. Mater.* **9**, 676–684 (2010).
11. Han, M. Y., Gao, X. H., Su, J. Z. & Nie, S. Quantum-dot-tagged microbeads for multiplexed optical coding of biomolecules. *Nat. Biotechnol.* **19**, 631–635 (2001).
12. Gao, X. H. *et al.* In vivo cancer targeting and imaging with semiconductor quantum dots. *Nat. Biotechnol.* **22**, 969–976 (2004).
13. Dong, A. G. *et al.* A Generalized ligand-exchange strategy enabling sequential surface functionalization of colloidal nanocrystals. *J. Am. Chem. Soc.* **133**, 998–1006 (2011).
14. Tu, N. N. & Wang, L. Y. Surface plasmon resonance enhanced upconversion luminescence in aqueous media for TNT selective detection. *Chem. Commun.* DOI:10.1039/C3CC43146K (2013).
15. Dubertret, B. *et al.* In vivo imaging of quantum dots encapsulated in phospholipid micelles. *Science* **298**, 1759–1762 (2002).
16. Park, J. *et al.* Ultra-large-scale syntheses of monodisperse nanocrystals. *Nat. Mater.* **3**, 891–895 (2004).
17. Chan, W. C. & Nie, S. Quantum dot bioconjugates for ultrasensitive nonisotopic detection. *Science* **281**, 2016–2018 (1998).
18. Bruchez, M. Jr., Moronne, M., Gin, P., Weiss, S. & Alivisatos, A. P. Semiconductor nanocrystals as fluorescent biological labels. *Science* **281**, 2013–2016 (1998).
19. Dubois, F., Mahler, B., Dubertret, B., Doris, E. & Mioskowski, C. A versatile strategy for quantum dot ligand exchange. *J. Am. Chem. Soc.* **129**, 482–483 (2007).
20. Kim, S. & Bawendi, M. G. Oligomeric ligands for luminescent and stable nanocrystal quantum dots. *J. Am. Chem. Soc.* **125**, 14652–14653 (2003).
21. Carion, O., Mahler, B., Pons, T. & Dubertret, B. Synthesis, encapsulation, purification and coupling of single quantum dots in phospholipid micelles for their use in cellular and in vivo imaging. *Nat. Protoc.* **2**, 2383–2390 (2007).
22. Liu, W. H. *et al.* Compact cysteine-coated CdSe(ZnCdS) quantum dots for in vivo applications. *J. Am. Chem. Soc.* **129**, 14530–14531 (2007).
23. Uyeda, H. T., Medintz, I. L., Jaiswal, J. K., Simon, S. M. & Mattoussi, H. Synthesis of compact multidentate ligands to prepare stable hydrophilic quantum dot fluorophores. *J. Am. Chem. Soc.* **127**, 3870–3878 (2005).
24. Stewart, M. H. *et al.* Multidentate poly(ethylene glycol) ligands provide colloidal stability to semiconductor and metallic nanocrystals in extreme conditions. *J. Am. Chem. Soc.* **132**, 9804–9813 (2010).
25. Susumu, K. *et al.* Enhancing the stability and biological functionalities of quantum dots via compact multifunctional ligands. *J. Am. Chem. Soc.* **129**, 13987–13996 (2007).
26. Hu, X. G. & Gao, X. H. Silica-polymer dual layer-encapsulated quantum dots with remarkable stability. *ACS Nano* **4**, 6080–6086 (2010).
27. Lu, Z. D. *et al.* Direct assembly of hydrophobic nanoparticles to multifunctional structures. *Nano Lett.* **11**, 3404–3412 (2011).
28. Yu, W. W. *et al.* Forming biocompatible and nonaggregated nanocrystals in water using amphiphilic polymers. *J. Am. Chem. Soc.* **129**, 2871–2879 (2007).
29. Pellegrino, T. *et al.* Hydrophobic nanocrystals coated with an amphiphilic polymer shell: a general route to water soluble nanocrystals. *Nano Lett.* **4**, 703–707 (2004).
30. Chen, H. Y. *et al.* Encapsulation of single small gold nanoparticles by diblock copolymers. *Chem Phys Chem* **9**, 388–392 (2008).
31. Deng, M. L., Tu, N. N., Bai, F. & Wang, L. Y. Surface functionalization of hydrophobic nanocrystals with one particle per micelle for bioapplications. *Chem. Mat.* **24**, 2592–2597 (2012).
32. Fan, H. Y. *et al.* Self-assembly of ordered, robust, three-dimensional gold nanocrystal/silica arrays. *Science* **304**, 567–571 (2004).
33. Bai, F. *et al.* A versatile bottom-up assembly approach to colloidal spheres from nanocrystals. *Angew. Chem.-Int. Edit.* **46**, 6650–6653 (2007).
34. Hu, S. H. & Gao, X. H. Nanocomposites with spatially separated functionalities for combined imaging and magnetolytic therapy. *J. Am. Chem. Soc.* **132**, 7234–7237 (2010).
35. Zhao, Y. Y., Ma, Y. X., Li, H. & Wang, L. Y. Composite QDs@MIP nanospheres for specific recognition and direct fluorescent quantification of pesticides in aqueous media. *Anal. Chem.* **84**, 386–395 (2012).
36. Ma, Y. X., Li, H. & Wang, L. Y. Magnetic-luminescent bifunctional nanosensors. *J. Mater. Chem.* **22**, 18761–18767 (2012).
37. Ma, Y. X., Li, H., Peng, S. & Wang, L. Y. Highly selective and sensitive fluorescent paper sensor for nitroaromatic explosive detection. *Anal. Chem.* **84**, 8415–8421 (2012).
38. Wang, L. Y. *et al.* Carboxylic acid enriched nanospheres of semiconductor nanorods for cell imaging. *Angew. Chem. -Int. Edit.* **47**, 1054–1057 (2008).
39. Sen, T. & Bruce, I. J. Surface engineering of nanoparticles in suspension for particle based bio-sensing. *Sci. Rep.* **2**, 564; DOI: 10.1038/srep00564 (2012).
40. Takahashi, H. *et al.* Modification of gold nanorods using phospatidylcholine to reduce cytotoxicity. *Langmuir* **22**, 2–5 (2006).
41. Alkilany, A. M. *et al.* Cellular uptake and cytotoxicity of gold nanorods: molecular origin of cytotoxicity and surface effects. *Small* **5**, 701–708 (2009).
42. Kang, H. S., Yang, S. R., Kim, J. D., Han, S. H. & Chang, I. S. Effects of grafted alkyl groups on aggregation behavior of amphiphilic poly(aspartic acid). *Langmuir* **17**, 7501–7506 (2001).
43. Koga, H. *et al.* Fluorescent nanoparticles consisting of lipopeptides and fluorescein-modified polyanions for monitoring of protein kinase activity. *Bioconjugate Chem.* **22**, 1526–1534 (2011).
44. Yang, H. M. *et al.* Poly(amino acid)-coated iron oxide nanoparticles as ultra-small magnetic resonance probes. *J. Mater. Chem.* **19**, 4566–4574 (2009).
45. Uchida, H. *et al.* Odd-even effect of repeating aminoethylene units in the side chain of N-substituted polyaspartamides on gene transfection profiles. *J. Am. Chem. Soc.* **133**, 15524–15532 (2011).
46. He, H., Xie, C. & Ren, J. Nonbleaching fluorescence of gold nanoparticles and its applications in cancer cell imaging. *Anal. Chem.* **80**, 5951–5957 (2008).
47. Li, J. L. *et al.* One-pot synthesis of aptamer-functionalized silver nanoclusters for cell-type-specific imaging. *Anal. Chem.* **84**, 4140–4146 (2012).
48. Lee, R. J. & Low, P. S. Folate-mediated tumor cell targeting of liposome-entrapped doxorubicin in vitro. *Biochim. Biophys. Acta* **1233**, 134–44 (1995).

Acknowledgments

Author contributions

S.H. carried out the experiments, analyzed and discussed the data. M.B. finished some fabrication of hydrophilic nanoparticles. L.Y.W. analyzed and discussed the data. S.H. and L.Y.W. prepared and revised the paper.

Additional information

Supplementary information accompanies this paper at http://www.nature.com/scientificreports

Competing financial interests: The authors declare no competing financial interests.

How to cite this article: Huang, S., Bai, M. & Wang, L. General and Facile Surface Functionalization of Hydrophobic Nanocrystals with Poly(amino acid) for Cell Luminescence Imaging. *Sci. Rep.* **3**, 2023; DOI:10.1038/srep02023 (2013).